



THE UNIVERSITY *of* EDINBURGH

Edinburgh Research Explorer

Versatile Locomotion by Integrating Ankle, Hip, Stepping, and Height Variation Strategies

Citation for published version:

Ding, J, Xin, S, Lam, TL & Vijayakumar, S 2021, Versatile Locomotion by Integrating Ankle, Hip, Stepping, and Height Variation Strategies. in *2021 IEEE International Conference on Robotics and Automation (ICRA)*. Institute of Electrical and Electronics Engineers, pp. 2957-2963, 2021 IEEE International Conference on Robotics and Automation, Xi'an, China, 30/05/21. <https://doi.org/10.1109/ICRA48506.2021.9561130>

Digital Object Identifier (DOI):

[10.1109/ICRA48506.2021.9561130](https://doi.org/10.1109/ICRA48506.2021.9561130)

Link:

[Link to publication record in Edinburgh Research Explorer](#)

Document Version:

Peer reviewed version

Published In:

2021 IEEE International Conference on Robotics and Automation (ICRA)

General rights

Copyright for the publications made accessible via the Edinburgh Research Explorer is retained by the author(s) and / or other copyright owners and it is a condition of accessing these publications that users recognise and abide by the legal requirements associated with these rights.

Take down policy

The University of Edinburgh has made every reasonable effort to ensure that Edinburgh Research Explorer content complies with UK legislation. If you believe that the public display of this file breaches copyright please contact openaccess@ed.ac.uk providing details, and we will remove access to the work immediately and investigate your claim.



Versatile Locomotion by Integrating Ankle, Hip, Stepping, and Height Variation Strategies

Jiatao Ding^{1*}, Songyan Xin², Tin Lun Lam^{1,3}, Sethu Vijayakumar^{2,4}

Abstract—Stable walking in real-world environments is a challenging task for humanoid robots, especially when considering the dynamic disturbances, e.g., caused by external perturbations that may be encountered during locomotion. The varying nature of disturbance necessitates high adaptability. In this paper, we propose an enhanced Nonlinear Model Predictive Control (NMPC) approach for robust and adaptable walking – we term it versatile locomotion, by limiting both the Center of Pressure (CoP) and Divergent Component of Motion (DCM) movements. Due to utilization of the Nonlinear Inverted Pendulum plus Flywheel model, the robot is endowed with the capabilities of CoP manipulation (if equipped with finite-sized feet), step location adjustment, upper body rotation, and vertical height variation. Considering the feasibility constraints, especially the usage of relaxed CoP constraints, the NMPC scheme is established as a Quadratically Constrained Quadratic Programming problem, which is solved efficiently by Sequential Quadratic Programming with enhanced solvability. Simulation experiments demonstrate the effectiveness of our method to recruit optimal hybrid strategies in order to realize versatile locomotion, for the robot with finite-sized or point feet.

I. INTRODUCTION

A versatile walking skill is highly desired for humanoid robots to operate in real-world environments. This demands robustness against dynamic disturbances, including modelling errors and external disturbances, and adaptability to different tasks, such as climbing stairs and crouching pass low passages. To this end, schemes that make use of various balance strategies such as the ankle, hip, stepping, and height variation strategies [1] (see Fig. 1) have been developed by the robotics community in recent years.

In [2], the ankle, hip and stepping strategies were integrated in a Nonlinear Model Predictive Control (NMPC) framework, leading to a time-consuming optimization process. To address this issue, time-efficient algorithms were developed in [3]–[5]. However, [2]–[5] assumed a constant plane for the Center of Mass (CoM) motion, which could not meet the height variation demand in particular cases, such as walking in the space with height limitation. To alleviate this limitation, the work in [6] proposed a measurement-based tracking controller, realizing CoM height variation and angular momentum variation (upper body rotation). In this

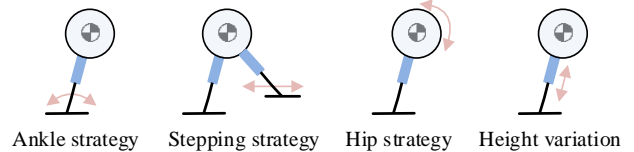


Fig. 1. Commonly-used balance strategies for versatile walking. Note that the ankle strategy is unavailable for a robot equipped with point feet.

way, the ankle, hip, and height variation strategies were utilized. Afterwards, the work in [7] and [8] individually proposed a linear MPC approach to deal with the upper body rotation and vertical height variation simultaneously, where merely tracked the offline-tuned height trajectory. Recently, the work in [9] used the Virtual-mass-ellipsoid Inverted Pendulum model and introduced a Quadratic Programming (QP) approach for solving time-varying height trajectory and upper body rotation angles. Nevertheless, [6]–[9] did not have the capability to adjust the footsteps. In contrast, the work in [10] proposed an NMPC approach for step location adjustment and height variation, where the ankle strategy was also integrated. Nevertheless, to the best of our knowledge, [10] did not take the upper body rotation into account.

Thus, the above studies failed to combine the ankle, stepping, hip, and height variation strategies in a unified way, limiting the robustness against disturbances. One example is that the step location can not be adjusted for rejecting extreme external pushes in [6]–[9]. Besides, the lack of access to some balance strategies weakens the adaptability to various scenarios. For example, it is hard to use the methods in [2]–[5] for climbing large staircases or walking in a space with height limitation.

In this paper, we propose an NMPC approach for versatile locomotion where the nonlinear Inverted Pendulum plus Flywheel (IPF) model is used to account for the effect of the height variation and the change of angular momentum. By customizing the cost function, the ankle (if allowable), stepping (footstep adjustment in this paper), hip, and height variation strategies are integrated. To guarantee the stability, the Center of Pressure (CoP) movement and Divergent Component of Motion (DCM) offset are both constrained. Through formulating the nonlinear issue as a Quadratically Constrained QP (QCQP) problem, it is solved fast by Sequential QP (SQP). The contribution is three-fold:

- 1) Complying with the hybrid stability criteria, the ankle (if allowable), stepping, hip, and height variation strategies are incorporated in a unified NMPC framework by employing the nonlinear IPF model;
- 2) By tuning weight coefficients, each balance strategy

This work is supported by the Shenzhen Institute of Artificial Intelligence and Robotics for Society (AIRS, 2019-ICP002) and the EPSRC UK RAI Hub in Future AI and Robotics for Space (FAIR-SPACE, EP/R026092/1)

¹ Authors are with the Shenzhen Institute of Artificial Intelligence and Robotics for Society (AIRS), Shenzhen, China.

² Authors are with School of Informatics, University of Edinburgh, Edinburgh, United Kingdom.

³ Author is with the Chinese University of Hong Kong, Shenzhen.

⁴ Author is a visiting researcher with AIRS.

*Corresponding author is Jiatao Ding (dingjiatao@cuhk.edu.cn)

can be activated flexibly, realizing versatile walking for robots equipped with finite-sized or point feet;

- 3) Formulating the enhanced NMPC by taking the acceleration as the control input allows it to be solved efficiently, meeting the real-time requirement.

The early results were presented in [11] and was employed in [12]. Compared with the preliminary version, the current paper is significantly improved by providing the following characteristics: i) the soft constraints on the CoP movement are adopted to enhance the solvability of NMPC, ii) the DCM is constrained to guarantee the walking stability, and the NMPC approach is extended to the robot equipped with point feet, iii) a reduced-order prediction model is employed to achieve higher time efficiency.

This paper is organized as follows. Section II introduces the background. Section III states the problem formulation. Section IV discusses the experimental results, and section V concludes our work.

II. BACKGROUND

A. Nonlinear IPF dynamics

To reduce the computing burden, reduced-order models can be employed for gait generation, among which the Linear Inverted Pendulum (LIP) model [13], the linear IPF model [14] and the Variable-height Inverted Pendulum (VHIP) model [15] have been recognized. However, the LIP model assumes a constant plane for CoM motion, and can not take the upper body rotation into account. Although the change of angular momentum is characterized by the rotation of a flywheel using the linear IPF model, the height variation can not be addressed. In contrast, the VHIP model can tackle the height variation but does not account for the body rotation.

To alleviate the above limitations, the nonlinear IPF model is adopted, assuming 1) the flywheel has rotational inertia, 2) legs are mass-less and telescopic, 3) the CoM is located at the hip joint, 4) the CoM can move in 3D space, as depicted in Fig. 2 [16]. As a result, the CoP is determined by¹

$$\begin{aligned} p_x &= c_x - \frac{c_z - d_z}{g + \ddot{c}_z} \ddot{c}_x - \frac{\dot{L}_y}{m(g + \ddot{c}_z)}, \text{ where } \dot{L}_y = I_y \ddot{\theta}_p, \\ p_y &= c_y - \frac{c_z - d_z}{g + \ddot{c}_z} \ddot{c}_y + \frac{\dot{L}_x}{m(g + \ddot{c}_z)}, \text{ where } \dot{L}_x = I_x \ddot{\theta}_r, \end{aligned} \quad (1)$$

where $[p_x, p_y]^T$, $[c_x, c_y, c_z]^T$ and $[d_x, d_y, d_z]^T$ denote the position of CoP, CoM, and stance foot, respectively. $[L_x, L_y]^T$ and $[\theta_r, \theta_p]^T$ denote the angular momentum and upper body rotation angle around x - and y - axis (x - and y - axis separately point to the forward and left direction). $[\ddot{c}_x, \ddot{c}_y, \ddot{c}_z]^T$, $[\ddot{\theta}_r, \ddot{\theta}_p]^T$, and $[\dot{L}_x, \dot{L}_y]^T$ denote the CoM acceleration, angular acceleration, and the change rate of angular momentum, respectively. $[I_x, I_y]^T$ denotes the constant moment of inertia. m is the robot mass and g is the gravitational acceleration.

¹To the best of our knowledge, the dynamics equations have been introduced in [16]. Recently, the work in [9] introduces the Virtual-mass-ellipsoid inverted pendulum that presents the same dynamical properties.

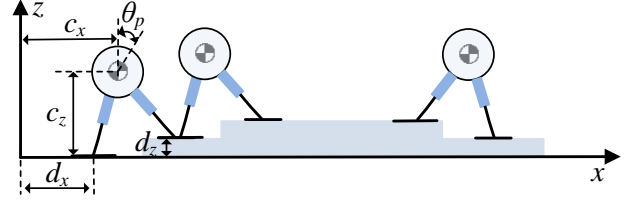


Fig. 2. The nonlinear IPF walks across uneven terrains.

B. CoP and DCM constraints

Stable walking can be realized by controlling the CoP movement. In [11], we expect the CoP calculated using (1) to fall within the support region. However, when the sole keeps the surface contact with the ground, the CoP may be able to exist beyond the support polygon [17]. Furthermore, to build an intrinsically stable mpc, the additional CoP constraints should be considered when formulating the prediction problem [18]. However, it would be very complicate to extract this kind of condition, especially its explicit expression when using the nonlinear IPF model. In this work, we adopt the soft CoP constraints to enhance the solvability. In this way, we can still employ the nonlinear IPF dynamics to account for the vertical height variation and upper body rotation.

Another interpretation is that the usage of hard CoP constraints maybe too stringent for dynamic walking since it limits both the convergent and divergent components of motion [19]–[21]. Actually, by merely the controlling DCM, the stable locomotion can be realized. In [22], the N -step capturability conditions for inverted pendulum models with constant height were derived. Recently, the capturability condition for the VHIP was derived in [15]. However, to the best of our knowledge, the method in [15] totally abandoned the CoP constraints and is hard to account for the hip strategy. Although the work in [23] taken the angular momentum change into account, it is hard to be used in a real-time fashion due to the computing complexity. In terms of viability analysis, [21] proves that by restricting the DCM offset, defining as the deviation between final DCM position of the current step and the next step location, the LIP can maintain stability.

For the sake of simplification, the LIP-based DCM offset bounds [21], which equals to the ∞ -step capture condition [22], are used for DCM control, which can be seen as the complementary conditions for the slack CoP constraints. Although the capturability region of the LIP is a subset of that of the IPF, the LIP-based ∞ -step capturability enables the robot to maintain the balance in most cases. Furthermore, the DCM offset bounds can be easily applied on the robot with point feet, improving the generality of our work.

III. NMPC FORMULATION

This section introduces the NMPC formulation. Particularly, we highlight the improvements with respect to [11].

A. Reduced-order prediction model

Differing from traditional MPC strategies that take the jerk of each motion component as the control input [2], [10],

[11], [24], [25], this work uses the acceleration. Assuming constant accelerations over the time interval Δt , the system state at $t_{(k+1)}$ is computed as

$$\hat{\mathbf{x}}_{(k+1)} = \mathbf{A}\hat{\mathbf{x}}_{(k)} + \mathbf{B}\ddot{\mathbf{x}}_{(k)}, \quad (2)$$

where $\hat{\mathbf{x}}_{(k)} = [x_{(k)}, \dot{x}_{(k)}]^T$ ($x \in \{c_x, c_y, c_z, \theta_r, \theta_p\}$) is the current state, $\ddot{\mathbf{x}}_{(k)}$ is the current acceleration, i.e., control input. And \mathbf{A} and \mathbf{B} are defined as

$$\mathbf{A} = \begin{bmatrix} 1 & \Delta t \\ 0 & 1 \end{bmatrix}, \quad \mathbf{B} = \begin{bmatrix} \frac{1}{2}\Delta t^2 \\ \Delta t \end{bmatrix}.$$

Based on (2), the position and velocity of each channel over the prediction horizon (of length N_h) are predicted as

$$\begin{aligned} \mathbf{x}_{(k)} &= \mathbf{P}_{ps}\hat{\mathbf{x}}_{(k)} + \mathbf{P}_{pu}\ddot{\mathbf{x}}_{(k)}, \\ \dot{\mathbf{x}}_{(k)} &= \mathbf{P}_{vs}\hat{\mathbf{x}}_{(k)} + \mathbf{P}_{vu}\ddot{\mathbf{x}}_{(k)}, \end{aligned} \quad (3)$$

where $\mathbf{x}_{(k)} = [x_{(k+1)}, \dots, x_{(k+N_h)}]^T$, $\dot{\mathbf{x}}_{(k)} = [\dot{x}_{(k+1)}, \dots, \dot{x}_{(k+N_h)}]^T$, $\ddot{\mathbf{x}}_{(k)} = [\ddot{x}_{(k+1)}, \dots, \ddot{x}_{(k+N_h)}]^T$. $\mathbf{x} \in \{c_x, c_y, c_z, \theta_r, \theta_p\}$ collect the future CoM position and body rotation angle. \mathbf{P}_{ps} , \mathbf{P}_{pu} , \mathbf{P}_{vs} and \mathbf{P}_{vu} can be obtained by computing (2) recursively.

B. Cost function

We attempt to minimize the tracking errors of the CoM position, body rotation angles, and step locations while regulating the velocity of each motion channel. Besides, the control inputs are also penalized. Thus, the cost function is

$$\begin{aligned} f = \sum_{\mathbf{x}} \left\{ \frac{\alpha_{\mathbf{x}}}{2} \|\mathbf{x}_{(k)} - \mathbf{x}_{(k)}^{\text{ref}}\|^2 + \frac{\beta_{\mathbf{x}}}{2} \|\dot{\mathbf{x}}_{(k)}\|^2 + \frac{\gamma_{\mathbf{x}}}{2} \|\ddot{\mathbf{x}}_{(k)}\|^2 \right\} \\ + \sum_{\mathbf{d}} \frac{\delta_{\mathbf{d}}}{2} \|\mathbf{d}_{(k)} - \mathbf{d}_{(k)}^{\text{ref}}\|^2 + \sum_{\xi} \frac{\lambda_{\xi}}{2} \|\xi_{(k)}\|^2 \end{aligned} \quad (4)$$

where $\alpha_{\mathbf{x}}$, $\beta_{\mathbf{x}}$, $\gamma_{\mathbf{x}}$, $\delta_{\mathbf{d}}$ and λ_{ξ} denote the penalties of position tracking, velocity variation, acceleration variation, step location tracking and CoP relaxation terms, respectively. $\mathbf{x}_{(k)}^{\text{ref}} = [x_{(k+1)}^{\text{ref}}, \dots, x_{(k+N_h)}^{\text{ref}}]^T$ are the reference states. $\mathbf{d}_{(k)}$ and $\mathbf{d}_{(k)}^{\text{ref}}$ are the actual and reference future step locations, e. g. $\mathbf{d}_{(k)}^{\text{ref}} = [d_{(k,1)}^{\text{ref}}, \dots, d_{(k,N_f)}^{\text{ref}}]^T$ ($\mathbf{d} \in \{d_x, d_y, d_z\}$). Note that we use $\bar{\mathbf{d}}_{(k)} = [d_{(k+1)}, \dots, d_{(k+N_h)}]^T$ denote footstep positions at different sampling times over the prediction horizon. N_f is the number of future step locations. $\xi \in \{\xi_{xl}, \xi_{xu}, \xi_{yl}, \xi_{yu}\}$ are the slack variables to formulate the soft CoP constraints.

At present, we choose the decision variables (\mathcal{X}) as

$$\mathcal{X}_{(k)} = [\ddot{c}_{x(k)}; \ddot{c}_{y(k)}; \ddot{c}_{z(k)}; \ddot{\theta}_r(k); \ddot{\theta}_p(k); \mathbf{d}_{x(k)}; \mathbf{d}_{y(k)}; \mathbf{d}_{z(k)}; \mathbf{\Upsilon}], \quad (5)$$

where $\mathbf{\Upsilon} = [\xi_{xl}, \xi_{xu}, \xi_{yl}, \xi_{yu}]^T$.

Using (4), the CoP position, step location, body rotation angle and CoM height can be adjusted. The expression of (4) can be obtained following the rationale in [11].

C. Reference movement

Normally, the reference roll and pitch angles are set to be zeros to keep the upper body upright. Besides, the reference CoM height are designed as the sum of the nominal pendulum height ($\mathbf{h}_c^{\text{ref}}$) and the reference step height ($\bar{\mathbf{d}}_{z(k)}^{\text{ref}}$).

That is, the reference CoM height ($c_{z(k)}^{\text{ref}}$) is defined as

$$c_{z(k)}^{\text{ref}} = \mathbf{h}_c^{\text{ref}} + \bar{\mathbf{d}}_{z(k)}^{\text{ref}}, \quad (6)$$

where $\mathbf{h}_c^{\text{ref}}$ is a constant vector (consisting of h_c^{ref}) which is determined by the physical structure. $\bar{\mathbf{d}}_{z(k)}^{\text{ref}}$ is determined by the surface height configuration, which is spanned from $\mathbf{d}_{z(k)}^{\text{ref}}$ (see (15)). Note that when walking through a passage with limited height, the $\mathbf{h}_c^{\text{ref}}$ can be adjusted, which would be demonstrated in Section IV-B.2.

As to the horizontal CoM movement, differing from [11] where the reference CoM trajectory fixed above the support center, this paper provides a better initial guess, by employing the LIP model with point contact. As revealed in [12], given the generated step location, the CoM trajectory can be easily obtained by solving a two-point boundary problem. During the current step (the i^{th} step), the reference forward CoM position during the remaining period is determined by

$$c_{x(k+j)}^{\text{ref}} = c_{x(k)}^{\text{ref}} \cosh(\omega_0 t_j) + \frac{\dot{c}_{x(k)}^{\text{ref}}}{\omega_0} \sinh(\omega_0 t_j), \quad 1 \leq j \leq k_i - k, \quad (7)$$

where $t_j = j\Delta t$. k_i corresponds to the ending time of the i^{th} step, $\sinh(\cdot)$ and $\cosh(\cdot)$ denote the hyperbolic sine and cosine function, respectively. $\omega_0 = \sqrt{g/h_c^{\text{ref}}}$ is the nominal natural frequency. $[c_{x(k)}^{\text{ref}}, \dot{c}_{x(k)}^{\text{ref}}]^T$ is the current CoM status reference, which is updated by using following boundaries:

$$c_{x(k)}^{\text{ref}} = c_{x(k)}, \quad \dot{c}_{x(k_i)}^{\text{ref}} = (\hat{d}_{x(k)} + d_{x(k,1)})/2, \quad (8)$$

where $c_{x(k)}$ denotes the current CoM position, $\hat{d}_{x(k)}$ denotes the current support center, $d_{x(k,1)}$ denotes the next step location (note $c_{x(k)}$, $\hat{d}_{x(k)}$ and $d_{x(k,1)}$ are generated by the last optimization loop), $c_{x(k_i)}^{\text{ref}}$ denotes the final CoM position reference of the current cycle.

The reference CoM trajectory for the future steps can also be solved, following the idea behind (7) and (8). Note that the utilization of (7) indicates that the reference CoP coincides with the support center, contributing to the stable locomotion.

D. Feasibility constraints

To guarantee the feasibility, this work considers the stability and physical constraints.

1) *Soft constraints on CoP movement*: To enhance the robot mobility and the NMPC solvability, this work uses soft CoP constraints:

$$\mathbf{p}_x^{\min} + \xi_{xl} \leq \mathbf{p}_{x(k)} - \bar{\mathbf{d}}_{x(k)} \leq \mathbf{p}_x^{\max} + \xi_{xu}, \quad (9)$$

where $\mathbf{p}_{x(k)}$ and $\bar{\mathbf{d}}_{x(k)}$ separately denote the sagittal CoP positions and step locations over the prediction horizon. $[\mathbf{p}_x^{\min}, \mathbf{p}_x^{\max}]^T$ denote the constant lower and upper CoP boundaries, which are determined by the foot size. ξ_{xl} and ξ_{xu} are the slack variable vectors spanned from ξ_{xl} and ξ_{xu} .

2) *Hard constraints on DCM offset*: The walking stability can be preserved by limiting the distance between the final DCM of the current (i^{th}) step and the next step location. Taking the forward motion as an example, we have

$$b_x^{\min} \leq (c_{x(k_i)} + \dot{c}_{x(k_i)}/\omega_0) - d_{x(k,1)} \leq b_x^{\max}, \quad (10)$$

where $(c_{x(k_i)} + \dot{c}_{x(k_i)})/\omega_0$ computes the final DCM position of the current step, b_x^{\max} and b_x^{\min} separately denote the upper and lower boundaries of the DCM offset.

The conditions given by (10) can be explained in terms of ∞ -step capturability of the LIP with point feet [22]. In current work, we assume a constant step period. Consequently, the DCM offset bounds are given as

$$b_x^{\max} = \frac{s_x^{\max}}{e^{\omega_0 T} - 1}, \quad b_x^{\min} = \frac{s_x^{\min}}{e^{\omega_0 T} - 1}, \quad (11)$$

where T is the step duration, s_x^{\max} and s_x^{\min} denote the maximal and minimal step length, respectively.

3) *Other physical limitations*: Feasibility constraints arisen from the limited actuation capability and physical configuration are also considered. Particularly, the constraints on the step location variation, body angle variation, hip torque and others are incorporated when formulating the NMPC problem. More details can be found in [11].

As a result, the enhanced NMPC is formulated as a QCQP problem, as expressed in the Appendix. Particularly, the quadratic CoP constraints are derived in Appendix A.

IV. EVALUATION

This section validates the effectiveness of the proposed approach by conducting simulation experiments on the CO-MAN humanoid robot (height: 0.945m, weight: 31kg) [26]. Particularly, the dynamical walking of a robot using the same physical property but equipped with point feet is also demonstrated – videos of all the results can be accessed at: <https://www.youtube.com/watch?v=I.DainHodcU>

A. IPF simulation

1) Robust gait generation for IPF with finite-sized feet:

In this section, the simulation on a nonlinear IPF with finite-sized feet is conducted where the robot was expected to climb 5cm high stairs from the 2nd to the 4th cycle. Besides, the horizontal push force lasting 0.1s was applied to the pelvis at 2s (forward 180N, leftward 100N). The step period is 0.8s and the default step length and step width are 0.15m and 0.145m. The weight coefficients are listed in Table II. Note that the λ_ξ s are set relatively high to minimize the CoP deviation. The generated motions are illustrated in Fig. 3.

Taking the motion during 3.2s~4.8s (from the 5th to the 7th step) as an example, the CoP is controlled near the support center (see Fig. 3(a)). Since there is no external push at this stage, the slack variables are suppressed below 0.1mm (see the partial enlarged drawing in Fig. 3(d)), which can be ignored compared with the size of feet plate. Besides, during 3.2s~4.8s, the robot tracks the reference height trajectory accurately, as illustrated in Fig. 3(b). Since the height variation strategy is integrated, the smooth transition is obtained when stepping across the stair. Furthermore, there is almost no footstep adjustment or body rotation at this stage, meaning that the utilization of the ankle strategy and height variation strategy helps to accomplish the walking task.

When the push force was applied at 2s, the robot modulated the CoP position. As illustrated in Fig. 3(a), the

CoP moves forward and leftward after 2s. To eliminate the state deviation caused by the external disturbance, the CoP during the whole 4th cycle and at the beginning of the 5th cycle is also modulated. Since the external disturbance is large enough, the upper body rotation is also employed, as illustrated in Fig. 3(c). Meanwhile, the robot adjusts the vertical height, as can be seen from Fig. 3(d).

It is worth mentioning that, although the slack variables increase a lot after 2s (e.g., ξ_{xu} reaches 0.3mm), they drop rapidly due to the change of the angular momentum and the height variation, as illustrated in Fig. 3(b)~(d). In this way, the CoP goes back to the support center as soon as possible. Furthermore, the generated final DCM state is always meeting the constraints given by (10) (see Fig. 3(a)), guaranteeing the walking stability.

Particularly, the step location variation is suppressed. Namely, when the stepping zone is limited, the robot can still maintain balance by employing the proposed NMPC approach. Note that a similar study can be found in [9]. However, to the best of our knowledge, [9] did not consider the footstep adjustment when formulating the problem.

2) Feasible gait generation for IPF with point feet:

Considering a robot with point feet, the step period is set to be 0.2s for fast stepping. In this case, the ankle strategy is unavailable. When using the hard CoP constraints (where no λ_ξ in Table II) is used, the NMPC strategy can not obtain the feasible solutions (the QP subproblem in each SQP loop is solved by the *quadprog* function in MATLAB 2017b). As illustrated in Fig. 4(a), the CoM trajectory diverges.

Using the soft CoP constraints (we set the λ_ξ smaller than α_x), the generated motions are plotted in Fig. 5. Due to the variation of slack variables, the CoP deviates from the support center (step location in Fig. 4(b)). Since the DCM offset is limited, the CoM trajectory converges. That is to say, the usage of soft CoP constraints enhances the recursive stability-termed as solvability in this article.

B. Dynamic simulation

In this section, dynamic simulations are conducted to demonstrate the robustness against dynamical disturbances, and the adaptability to complex environments as well.

1) *Push recovery when stepping in place*: To begin with, the push recovery behavior is analyzed by applying a horizontal external force to the pelvis at 2.4s when the CO-MAN robot is stepping in place. It turns out that more balance strategies need to be employed as the push force rises (please see the attached video). Using the enhanced NMPC strategy, the maximal push force the robot with finite-sized feet can recover rises from 100N to 125N by integrating hip strategy. When the stepping and height variation strategies are integrated, the robot can reject 155N push force.

Fig. 6 demonstrates the robot motion for rejecting 150N forward force. As illustrated in Fig. 6(a), the CoP moves forwards and backwards when the force is applied. As the footstep location varies, the generated CoM trajectory ('CoM-gen') is adjusted, constrained by the CoP and DCM motion. Besides, the upper body rotation (Fig. 6(b)) helps

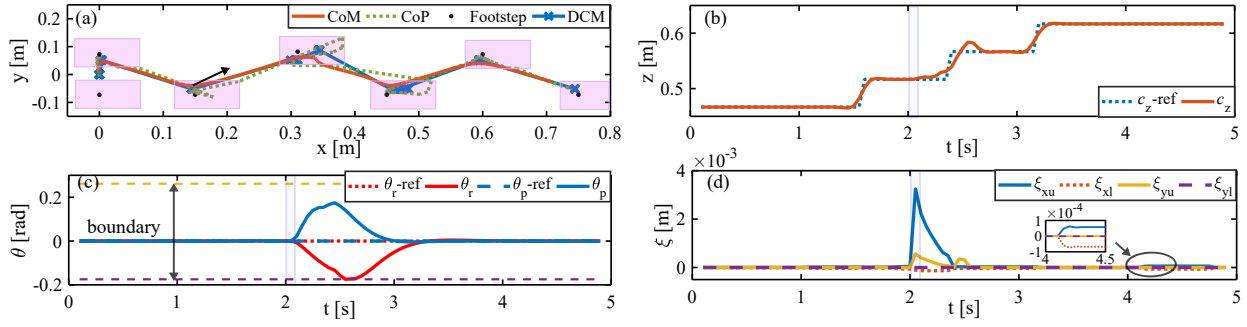


Fig. 3. The generated motion for the IPF with finite-sized feet. The pink blocks in (a) represent foot planes while the black arrow marks the direction of external push, shallow grey strips in (b), (c) and (d) mark the time duration when external force is applied. Note that the final DCM position of each step cycle is always calculated and plotted in (a).

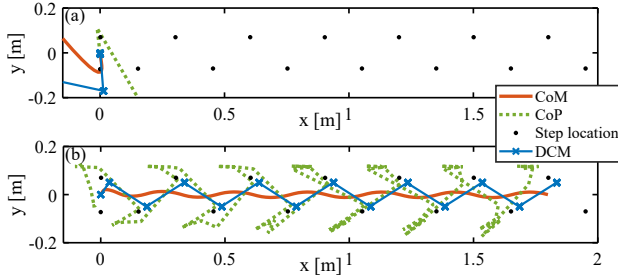


Fig. 4. Gait generation for the IPF with point feet (no support polygon for CoP movement). (a) plots the infeasible motions generated by the original NMPC using hard CoP constraints, (b) plots the feasible motions generated by the enhanced NMPC using soft CoP constraints. The step locations in (a) are the reference ones while the step locations in (b) are generated by the enhanced NMPC.

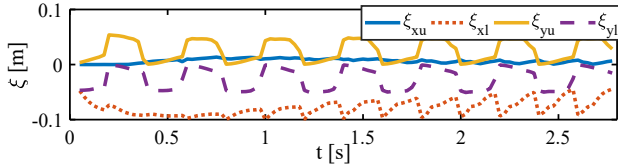


Fig. 5. Slack variables generated by the enhanced NMP.

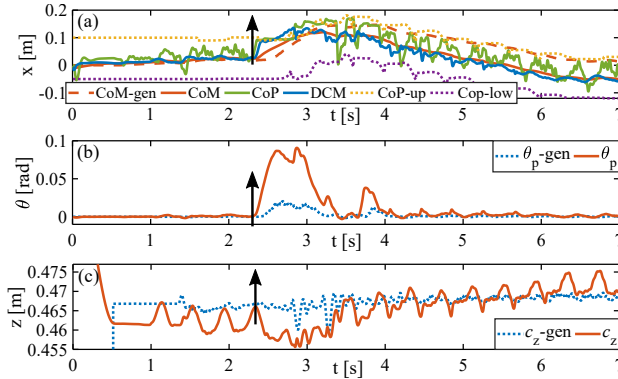


Fig. 6. Push recovery when stepping in place. The black arrows mark the time when external push is applied. ‘-gen’ denote the optimal trajectory generated by the NMPC.

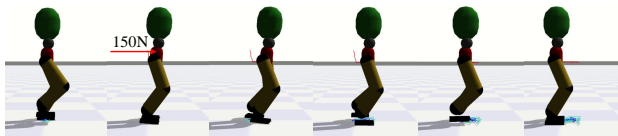


Fig. 7. The robot recovers from 150N external force.

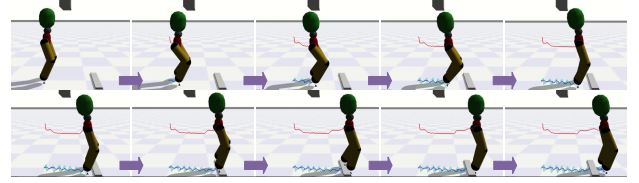


Fig. 8. The robot equipped with point feet passes by a composite scenario.

to reconcile the external push while the vertical height is changed to dissipate the excessive kinetic energy input by the disturbance (Fig. 6(c)). Based on the state feedback, the upper body rotation and CoM height are modified in real-time. Consequently, the robot returns to track the normal states after the push force vanishes.

The snapshots of walking motions are illustrated in Fig. 7. Note that the robot with point feet can also recover from external pushes due to the availability of step, hip and height variation strategies providing by this approach. For more details, please see the supplementary video.

2) *Stable walking with height limitation*: In real-world environments, the robot often meets the walking tasks demanding height variation. Taking the robot with point feet as an example, the robot first walks across a passage with shorter height (91cm high) and then climbs a 2cm tall staircase, as illustrated in Fig. 8.

To avoid the collision, the robot needs to reduce the total height at the first stage. In this case, the reference height trajectory is reduced by 4cm by adjusting h_c^{ref} . As a result, the robot successfully walks across the lower space, as illustrated in the first row in Fig. 8. After then, the robot climbs the stair by setting the step height to be 2cm, see the second row in Fig. 8. That is to say, our approach can obtain adaptable gaits by generating a time-varying height trajectory.

The similar test has also been conducted on a robot with finite-sized feet, which can be found in the attached video.

C. Computing efficiency

Similar to [11], we use the following terminal condition:

$$\begin{aligned} \text{Case 1: } \min(\mathbf{F}^m) &\leq \varepsilon \text{ where } \mathbf{F}_{(i)}^m = \max(\Delta \mathbf{x}_{(i)}), \text{ for } 1 \leq i \leq 8, \\ \text{Case 2: } n_k &\geq N_s, \end{aligned} \quad (12)$$

where $\Delta \mathbf{x}$, consisting of 8 blocks, is computed by the QP solver, $\mathbf{F}^m \in \mathfrak{R}^8$, n_k is the loop count of QP solver.

That is to say, there are two ways to terminate the SQP loop. The first way is that we judge the maximal absolute value ($F_{(i)}^m$) of each state channel ($\Delta \mathbf{x}_{(i)}$), including 3D CoM, 2D body inclination angle and 3D step location, over the prediction horizon. Then, we compare the minimum of the maximums with the threshold value (ε). The second way is to judge if the loop number goes beyond the limit.

We use the c++ library *QuadProg++* to solve the QP subproblem, where the active-set algorithm [27] is employed. For the test, the Δt is 0.1s and N_h is 10. With a 3.3 GHz quad-core CPU, we found that ε reduces as N_s increases, as listed in Table I. However, when N_s becomes larger than 3, the effect is dramatically weakened. On the other hand, the time cost keeps rising as the growth of N_s . Thus, for the real-time application, we choose $\varepsilon = 1 \times 10^{-8}$ and $N_s = 3$.

TABLE I
THRESHOLD VALUES AND COMPUTING TIME

Param.	N_s	1	2	3	4	5	6
ε		1×10^{-2}	2×10^{-6}	1×10^{-8}	4×10^{-9}	8×10^{-10}	2×10^{-10}
t [ms]		1.31	2.36	3.39	4.21	4.90	5.52
t [ms] ([11])		1.52	2.64	3.56	4.56	5.52	6.57

Compared with the preliminary version in [11], the number of decision variables of the enhanced NMPC increases by 4, due to the introduction of CoP slack variables. Besides, the number of the inequality constraints is also increased by 4 because of the utilization of DCM offset constraints. However, in this work, by using the accelerations as control inputs, the orders of coefficient matrices, e.g., \mathbf{A} and \mathbf{B} in (2) are reduced. Besides, the time cost for preparing the feasibility constraints, especially for the CoP constraints computing, is dramatically reduced, when compared (18) with the work in [11]. As a result, the enhanced NMPC needs less time cost than [11], as can be seen in Table I. Thus, the proposed scheme contributes to higher time efficiency.

V. CONCLUSION AND DISCUSSION

In this work, an enhanced NMPC approach is proposed for versatile locomotion. By using the nonlinear IPF model, the CoP modulation (if allowable), footstep adjustment, body rotation and height variation are integrated in a unified way. Complying with the hybrid stability criteria, the method can be applied on the robot with finite-sized feet or point feet.

One challenge is the automatic decision of weights for achieving optimal hybrid strategy. At present, the weight coefficients are tuned by hand. To overcome this drawback, one possible way is to employ learning-based methods to train the weight factors.

Another work is taking the step duration adaptation into account. As revealed in [21] and [28], the step timing modulation can highly enhance the gait robustness, which is our next focus.

TABLE II
WEIGHT COEFFICIENTS FOR IPF SIMULATION

α_{C_x}	$1 \times 10^4 / 1 \times 10^7$	α_{C_y}	$5 \times 10^3 / 5 \times 10^5$	α_{C_z}	$2 \times 10^7 / 1 \times 10^9$
α_{Θ_r}	$8 \times 10^3 / 5 \times 10^8$	α_{Θ_p}	$2 \times 10^4 / 5 \times 10^8$	β_{C_x}	100/10
β_{C_y}	100/10	β_{C_z}	100/10	β_{Θ_r}	100/10
β_{Θ_p}	100/10	γ_{C_x}	10/100	γ_{C_y}	10/100
γ_{C_z}	50/100	γ_{Θ_r}	10/100	γ_{Θ_p}	10/100
δ_{D_x}	$5 \times 10^7 / 5 \times 10^8$	δ_{D_y}	$1 \times 10^7 / 1 \times 10^9$	λ_ξ	$5 \times 10^8 / 1 \times 10^7$

APPENDIX

The NMPC is formulated as a in-homogeneous QCQP problem, which can be expressed as

$$\begin{aligned} \min_{\mathbf{X}} \quad & \mathbf{X}^T \mathbf{G} \mathbf{X} + 2\mathbf{g}^T \mathbf{X}, \\ \text{s.t.} \quad & \mathbf{X}^T \mathbf{V}_j \mathbf{X} + \mathbf{v}_j^T \mathbf{X} + \leq \sigma_j, j \in \{1, \dots, N_c\}, \end{aligned} \quad (13)$$

where $\mathbf{X} \in \mathbb{R}^{N_t}$ is the state vector, N_c and N_t denote the number of constraints and state variables, respectively. \mathbf{G} , $\mathbf{V}_j \in \mathbb{R}^{N_t \times N_t}$, $\mathbf{v}_j \in \mathbb{R}^{N_t}$, and $\sigma_j \in \mathbb{R}$ are the coefficients that specify the cost function and constraints.

A. Quadratic form of soft CoP constraints

At $t_{(k)}$, by defining the selection matrices, the predictive accelerations and step locations can be expressed as follows:

$$\begin{aligned} \mathbf{d}_{(k)} &= \mathbf{S}_d \mathbf{X}_{(k)}, \quad \mathbf{S}_d \in \mathbb{R}^{N_f \times N_t}, \\ \tilde{\mathbf{x}}_{(k)} &= \mathbf{S}_x \mathbf{X}_{(k)}, \quad \mathbf{S}_x \in \mathbb{R}^{N_h \times N_t}, \\ \tilde{\mathbf{x}}_{(k+i)} &= \mathbf{S}_i \tilde{\mathbf{x}}_{(k)}, \quad \mathbf{S}_i \in \mathbb{R}^{1 \times N_h}, i \in \{1, \dots, N_h\}. \end{aligned} \quad (14)$$

Besides, the step locations over the prediction horizon are generated by using the separated locations corresponding to the future walking cycles. That is,

$$\bar{\mathbf{d}}_{x(k)} = \mathbf{e}_{c(k)} \hat{\mathbf{d}}_{x(k)} + \mathbf{E}_{c(k)} \mathbf{d}_{x(k)}, \quad (15)$$

where $\hat{\mathbf{d}}_{x(k)}$ denotes the current support center, $\mathbf{e}_{c(k)}$ and $\mathbf{E}_{c(k)}$ are mapping matrix as defined in [24].

Then, the position of support foot is chosen as

$$d_{x(k+i)} = \mathbf{S}_i \bar{\mathbf{d}}_{x(k)}. \quad (16)$$

Focusing on the upper portion of CoP motion, we have:

$$\begin{aligned} (c_{x(k+i)} - d_{x(k+i)} - (p_x^{\max} + \xi_{xu}))(g + \ddot{c}_{z(k+i)}) \\ - (c_{z(k+i)} - d_{z(k+i)})\ddot{c}_{x(k+i)} - I_y \ddot{\theta}_p(k+i)/m \leq 0. \end{aligned} \quad (17)$$

Then, by substituting (3), (14) and (16) into (17), the quadratic form of ZMP constraints is:

$$\begin{aligned} \mathbf{V}_{p_{x(i)}} &= m(\mathbf{S}_{c_x}^T \mathbf{P}_{pu}^T \mathbf{S}_i^T \mathbf{S}_i \mathbf{S}_{c_z} - \mathbf{S}_{c_x}^T \mathbf{S}_i^T \mathbf{S}_i \mathbf{P}_{pu} \mathbf{S}_{c_z} - \mathbf{S}_{d_x}^T \mathbf{E}_{c(k)}^T \mathbf{S}_i^T \mathbf{S}_i \mathbf{S}_{c_z}), \\ \mathbf{v}_{p_{x(i)}} &= m(\hat{c}_{x(k)}^T \mathbf{P}_{ps}^T \mathbf{S}_i^T \mathbf{S}_i \mathbf{S}_{c_z} + g \mathbf{S}_i \mathbf{P}_{pu} \mathbf{S}_{c_x} - \hat{c}_{z(k)}^T \mathbf{P}_{ps}^T \mathbf{S}_i^T \mathbf{S}_i \mathbf{S}_{c_x} \\ &\quad + d_{z(k+i)}^{\text{ref}} \mathbf{S}_j \mathbf{S}_{c_x} - \hat{d}_{x(k)}^T \mathbf{e}_{c(k)}^T \mathbf{S}_i^T \mathbf{S}_i \mathbf{S}_{c_z} - g \mathbf{S}_i \mathbf{E}_{c(k)} \mathbf{S}_{d_x} \\ &\quad - (p_x^{\max} + \xi_{xu}) \mathbf{S}_i \mathbf{S}_{c_z})^T - (I_y \mathbf{S}_i \mathbf{S}_{\theta_p})^T, \\ \sigma_{p_{x(i)}} &= m g (\mathbf{S}_i (\mathbf{P}_{ps} \hat{c}_{x(k)} - \mathbf{e}_{c(k)} \hat{\mathbf{d}}_{x(k)}) - (p_x^{\max} + \xi_{xu})). \end{aligned} \quad (18)$$

B. Weight coefficients for NMPC solution

Table II lists the weight coefficients for the IPF simulation. Note that, for each term, the left is for the IPF with finite-sized feet while the right is for the IPF with point feet.

REFERENCES

- [1] C. McGreavy, K. Yuan, D. Gordon, K. Tan, W. J. Wolfslag, S. Vijayakumar, and Z. Li, "Unified push recovery fundamentals: Inspiration from human study," in *IEEE International Conference on Robotics and Automation*, 2020, pp. 876–882.
- [2] Z. Aftab, T. Robert, and P.-B. Wieber, "Ankle, hip and stepping strategies for humanoid balance recovery with a single model predictive control scheme," in *IEEE-RAS International Conference on Humanoid Robots*, 2012, pp. 159–164.
- [3] F. Nazemi, A. Yousefi-Koma, M. Khadiv *et al.*, "A reactive and efficient walking pattern generator for robust bipedal locomotion," in *RSI International Conference on Robotics and Mechatronics*, 2017, pp. 364–369.
- [4] H. Jeong, I. Lee, J. Oh, K. K. Lee, and J.-H. Oh, "A robust walking controller based on online optimization of ankle, hip, and stepping strategies," *IEEE Transactions on Robotics*, vol. 35, no. 6, pp. 1367–1386, 2019.
- [5] Y. Kojio, Y. Omori, K. Kojima, F. Sugai, Y. Kakiuchi, K. Okada, and M. Inaba, "Footstep modification including step time and angular momentum under disturbances on sparse footholds," *IEEE Robotics and Automation Letters*, vol. 5, no. 3, pp. 4907–4914, 2020.
- [6] J. Engelsberger and C. Ott, "Integration of vertical com motion and angular momentum in an extended capture point tracking controller for bipedal walking," in *IEEE-RAS International Conference on Humanoid Robots*, 2012, pp. 183–189.
- [7] J. Lack, "Integrating the effects of angular momentum and changing center of mass height in bipedal locomotion planning," in *IEEE-RAS International Conference on Humanoid Robots*, 2015, pp. 651–656.
- [8] M. Shafiee-Ashtiani, A. Yousefi-Koma, and M. Shariat-Panahi, "Robust bipedal locomotion control based on model predictive control and divergent component of motion," in *IEEE International Conference on Robotics and Automation*, 2017, pp. 3505–3510.
- [9] K. Guan, K. Yamamoto, and Y. Nakamura, "Virtual-mass-ellipsoid inverted pendulum model and its applications to 3d bipedal locomotion on uneven terrains," in *IEEE/RSJ International Conference on Intelligent Robots and Systems*, 2019, pp. 1401–1406.
- [10] K. Van Heerden, "Real-time variable center of mass height trajectory planning for humanoids robots," *IEEE Robotics and Automation Letters*, vol. 2, no. 1, pp. 135–142, 2017.
- [11] J. Ding, C. Zhou, S. Xin, X. Xiao, and N. Tsagarakis, "Nonlinear model predictive control for robust bipedal locomotion exploring com height and angular momentum changes," *arXiv preprint arXiv:1902.06770*, 2019.
- [12] J. Ding, C. Zhou, Z. Guo, X. Xiao, and N. Tsagarakis, "Versatile reactive bipedal locomotion planning through hierarchical optimization," in *IEEE International Conference on Robotics and Automation*, 2019, pp. 256–262.
- [13] S. Kajita, F. Kanehiro, K. Kaneko, K. Yokoi, and H. Hirukawa, "The 3d linear inverted pendulum mode: A simple modeling for a biped walking pattern generation," in *IEEE/RSJ International Conference on Intelligent Robots and Systems*, vol. 1, 2001, pp. 239–246.
- [14] J. Pratt, J. Carff, S. Drakunov, and A. Goswami, "Capture point: A step toward humanoid push recovery," in *IEEE-RAS international conference on humanoid robots*, 2006, pp. 200–207.
- [15] S. Caron, A. Escande, L. Lanari, and B. Mallein, "Capturability-based pattern generation for walking with variable height," *IEEE Transactions on Robotics*, vol. 36, no. 2, pp. 517–536, 2019.
- [16] S. Kajita, H. Hirukawa, K. Harada, and K. Yokoi, *Introduction to humanoid robotics*. Springer, 2014, vol. 101.
- [17] M. Vukobratović, B. Borovac, and D. Šurdilović, "Zero moment point-proper interpretation and new applications," in *IEEE-RAS International Conference on Humanoid Robots*, 2001, pp. 237–244.
- [18] N. Scianca, D. De Simone, L. Lanari, and G. Oriolo, "Mpc for humanoid gait generation: Stability and feasibility," *IEEE Transactions on Robotics*, vol. 36, no. 4, pp. 1171–1188, 2020.
- [19] J. Engelsberger, C. Ott, and A. Albu-Schäffer, "Three-dimensional bipedal walking control using divergent component of motion," in *IEEE/RSJ International Conference on Intelligent Robots and Systems*, 2013, pp. 2600–2607.
- [20] T. Takenaka, T. Matsumoto, and T. Yoshiike, "Real time motion generation and control for biped robot-3 rd report: Dynamics error compensation," in *IEEE/RSJ International Conference on Intelligent Robots and Systems*, 2009, pp. 1594–1600.
- [21] M. Khadiv, A. Herzog, S. A. A. Moosavian, and L. Righetti, "Walking control based on step timing adaptation," *IEEE Transactions on Robotics*, vol. 36, no. 3, pp. 629–643, 2020.
- [22] T. Koolen, T. De Boer, J. Rebula, A. Goswami, and J. Pratt, "Capturability-based analysis and control of legged locomotion, part 1: Theory and application to three simple gait models," *The international journal of robotics research*, vol. 31, no. 9, pp. 1094–1113, 2012.
- [23] M. A. Posa, T. Koolen, and R. L. Tedrake, "Balancing and step recovery capturability via sums-of-squares optimization," in *Robotics: Science and Systems*, 2017, pp. 12–16.
- [24] H. Diedam, D. Dimitrov, P.-B. Wieber, K. Mombaur, and M. Diehl, "Online walking gait generation with adaptive foot positioning through linear model predictive control," in *IEEE/RSJ International Conference on Intelligent Robots and Systems*, 2008, pp. 1121–1126.
- [25] C. Brasseur, A. Sherikov, C. Collette, D. Dimitrov, and P.-B. Wieber, "A robust linear mpc approach to online generation of 3d biped walking motion," in *IEEE-RAS International Conference on Humanoid Robots*, 2015, pp. 595–601.
- [26] N. G. Tsagarakis, S. Morfeý, G. M. Cerda, L. Zhibin, and D. G. Caldwell, "Compliant humanoid coman: Optimal joint stiffness tuning for modal frequency control," in *IEEE International Conference on Robotics and Automation*, 2013, pp. 673–678.
- [27] D. Goldfarb and A. Idnani, "A numerically stable dual method for solving strictly convex quadratic programs," *Mathematical programming*, vol. 27, no. 1, pp. 1–33, 1983.
- [28] J. Ding, X. Xiao, N. Tsagaraki, and Y. Huang, "Robust gait synthesis combining constrained optimization and imitation learning," in *IEEE/RSJ International Conference on Intelligent Robots and Systems*, 2020, pp. 3473–3480.